Molecular Biology of the Cell
Vol. 13, 238–250, January 2002

Caveolae Are Highly Immobile Plasma Membrane Microdomains, Which Are not Involved in Constitutive Endocytic Trafficking[V]

Peter Thomsen, Kirstine Roepstorff, Martin Stahlhut, and Bo van Deurs*

Structural Cell Biology Unit, Department of Medical Anatomy, The Panum Institute, DK-2200 Copenhagen N, Denmark

Submitted June 22, 2001; Revised September 21, 2001; Accepted October 10, 2001
Monitoring Editor: Howard Riezman

To investigate whether caveolae are involved in constitutive endocytic trafficking, we expressed N- and C-terminally green fluorescent protein (GFP)-tagged caveolin-1 fusion proteins in HeLa, A431, and Madin-Darby canine kidney cells. The fusion proteins were shown by immunogold labeling to be sorted correctly to caveolae. By using confocal microscopy and photobleaching techniques, it was found that although intracellular structures labeled with GFP-tagged caveolin were dynamic, GFP-labeled caveolae were very immobile. However, after incubation with methyl-β-cyclodextrin, distinct caveolae disappeared and the mobility of GFP-tagged caveolin in the plasma membrane increased. Treatment of cells with cytochalasin D caused lateral movement and aggregation of GFP-labeled caveolae. Therefore, both cholesterol and an intact actin cytoskeleton are required for the integrity of GFP-labeled caveolae. Moreover, stimulation with okadaic acid caused increased mobility and internalization of the labeled caveolae. Although the calculated mobile fraction (for $t = \infty$) of intracellular, GFP-tagged caveolin-associated structures was 70–90%, GFP-labeled caveolae in unstimulated cells had a mobile fraction of $<20\%$, a value comparable to that previously reported for E-cadherin in junctional complexes. We therefore conclude that caveolae are not involved in constitutive endocytosis but represent a highly stable plasma membrane compartment anchored by the actin cytoskeleton.

INTRODUCTION

Caveolae are 50–100-nm invaginated plasma membrane domains present in many cell types. They are enriched in glycosphingolipids and cholesterol and characterized by the presence of the integral membrane protein caveolin. Caveolin-1 and -2 are ubiquitously expressed, whereas a third member of the caveolin family, caveolin-3, is found in muscle tissue (Parton, 1996; Anderson, 1998; Kurzchalia and Parton, 1999; Smart *et al.*, 1999). Caveolin and caveolae seem to play a role in many different cellular processes. For instance, cholesterol transport and homeostasis involve caveolin and caveolae (Fielding and Fielding, 1997, 2000; Ikonen and Parton, 2000; van Meer, 2001) and caveolin was recently found on the surface of cytoplasmic lipid droplets (Fujimoto *et al.*, 2001; Ostermeyer *et al.*, 2001; Pol *et al.*, 2001) and in secreted lipoprotein particles (Liu *et al.*, 1999). Caveolin and caveolae also seem to be important for, e.g., nitric oxide-, calcium-, H-Ras-, and nerve growth factor signaling (Huang *et al.*, 1999; Isshiki and Anderson, 1999; Roy *et al.*, 1999; Smart *et al.*, 1999; Bucci *et al.*, 2000b; Dessy *et al.*, 2000; Ranzani *et al.*, 2000; Stahlhut *et al.*, 2000). Furthermore, a relationship between cell adhesion via integrins and caveolin signaling has been indicated (Wary *et al.*, 1996, 1998; Wei *et al.*, 1999).

In addition, various stimuli can lead to internalization of caveolae, and the multifaceted role of caveolae in various endocytic processes is in fact one of the most remarkable features of these membrane domains. Thus, after binding of simian virus 40 to major histocompatibility complex class I molecules on the cell surface, the virus particles become internalized in caveolae to be transported to the endoplasmic reticulum via caveosomes, thereby bypassing the degradative endosomal-lysosomal route (Stang *et al.*, 1997; Parton and Lindsay, 1999; Pelkmans *et al.*, 2001). This process is stimulated by the virus, and it is even possible that the virus induces the formation of new caveolae tightly wrapping the

DOI: 10.1091/mbc.01–06-0317.
[V] Online version of this article contains video material in Figures 3, 5, 7, and 9. Online version available at www.molbiolcell.org.
* Corresponding author. E-mail address: b.v.deurs @mai.ku.dk.
Abbreviations used: FLIP, fluorescence loss in photobleaching; FRAP, fluorescence recovery in photobleaching; GFP, green fluorescent protein.

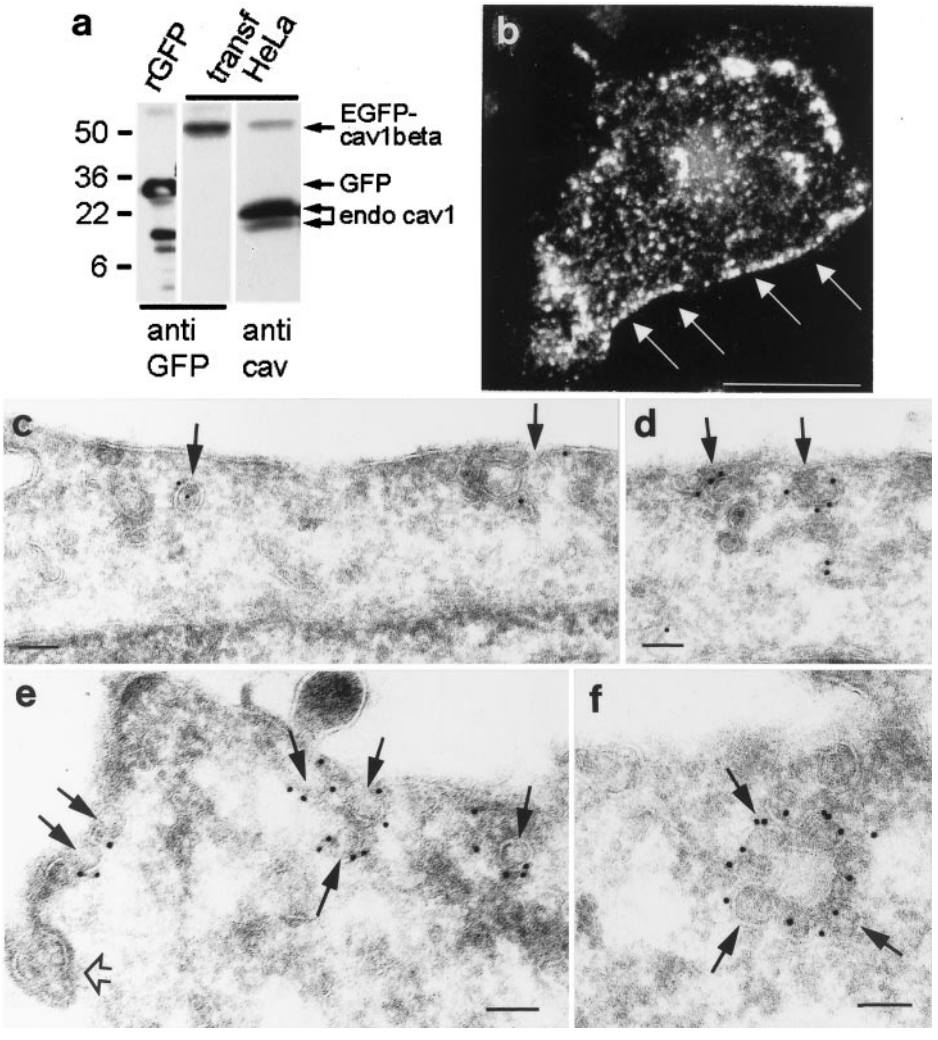

Figure 1. Expression of GFP-cav in transiently transfected cells. (a) Western blot showing that enhanced GFP-caveolin-1 β (EGFP-cav-1 β) expressed in HeLa cells can be detected as a single band of ~50 kDa by the use of a polyclonal anti-GFP antibody (anti-GFP) with no signs of degradation. Purified recombinant GFP (rGFP) served as a positive control. A polyclonal anti-caveolin-1 antibody (anti-cav) detects both the GFP-cav-1 β fusion protein and the endogenous caveolin-1 isoforms. (b) 3D reconstruction based on a stack of confocal images of a HeLa cell expressing GFP-cav-1 α. Fluorescent caveolae are in particular distinct at the cell periphery (arrows). Bar, 20 μm. (c–f) Ultracryo sections of GFP-cav-1 β-transfected MDCK cells (c and d) and GFP-cav-1 α transfected HeLa cells (e and f), immunogold labeled with a polyclonal antibody against GFP. The labeling is seen on caveolae (arrows), which sometimes form aggregates (f). An unlabeled clathrin-coated pit (open arrow) is seen in e. Bars, 100 nm.

individual virus particles. Caveolae also seem to be engaged in internalization of FimH-expressing *Escherichia coli* in macrophages and mast cells. This uptake is stimulated by binding of the bacterium to the GPI-anchored protein CD48 present in caveolae and subsequent recruitment and clustering of numerous caveolae, which eventually form an intracellular, bacterium-containing compartment (Shin *et al.*, 2000; Shin and Abraham, 2001). Another example of stimulated endocytosis of caveolae is the clustering and subsequent internalization of these structures caused by the phosphatase inhibitor okadaic acid (Parton *et al.*, 1994). Moreover, in endothelial cells, where caveolae are involved in transendothelial transport of, e.g., albumin, budding of caveolae or caveolae-derived membrane has to be stimuated by interaction of the albumin-docking protein pg60 with caveolin-1 and subsequent activation of downstream G_i-coupled *Src* kinase signaling (Minshall *et al.*, 2000). It is striking that stimulated caveolar endocytic trafficking often seems to bypass the conventional endocytic organelles, i.e., endosomes and lysosomes. The significance of this routing is at present unknown but it obviously protects invading "opportunistic" ligands from being degraded.

However, whether caveolae are also part of a constitutive endocytic pathway operating in parallel with the well-established clathrin-mediated endocytic pathway has remained elusive (van Deurs *et al.*, 1993; Kurzchalia and Parton, 1996; Stahlhut *et al.*, 2000; Pfeffer, 2001). In constitutive endocytosis, vesicles are formed without stimulation at a constant rate from the plasma membrane and what comes in is continuously replaced by a corresponding outgoing traffic from an intracellular pool of vesicles and coat proteins, as typified in clathrin-dependent endocytosis (Gaidarov *et al.*, 1999). The critical parameter for maintaining such a steady-state situation is the mobile fraction of the involved vesicles (or of their coat proteins). This mobile fraction has to be close to 100%. If the population of vesicles/coat proteins has a lower mobile fraction, constitutive endocytosis will in principle be impossible, because the plasma membrane will eventually be depleted for membrane and coat proteins.

To determine whether caveolae are actively involved in constitutive endocytosis or rather represent a largely immobile plasma membrane compartment, i.e., to determine the mobile fraction of caveolae, we expressed N- or C-terminally GFP-tagged caveolin fusion proteins in some widely used

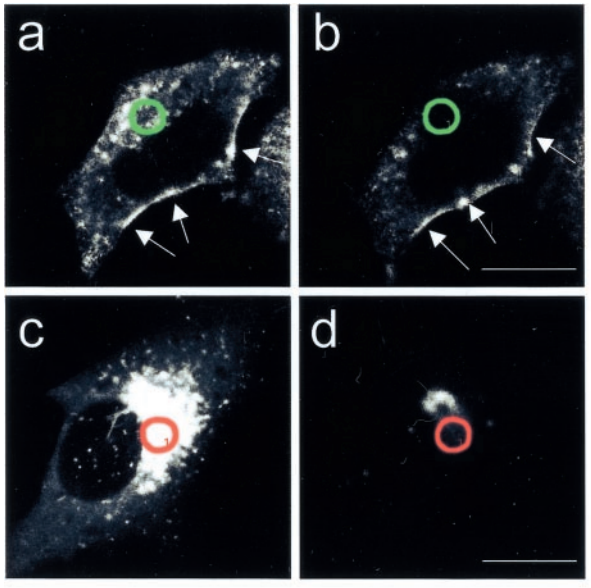

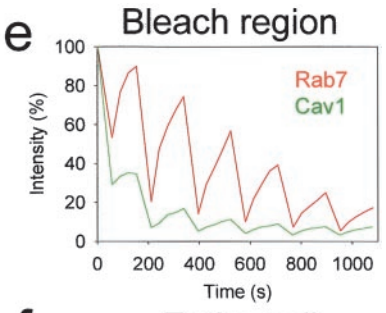

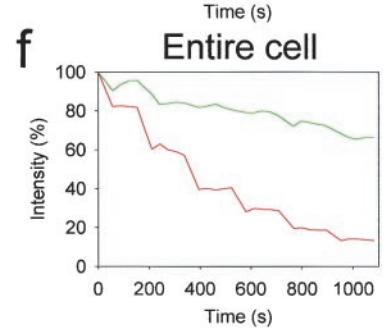

Figure 2. 4D-FLIP analysis of cells expressing GFP-cav and GFP-Rab7. (a and b) Indicated region (green circles) was bleached six times over ~18 min in a HeLa cell expressing GFP-cav-1 β. The two reconstructed 3D images show the fluorescence of the entire cell immediately before bleaching and at the end of the experiment. (c and d) Indicated region (red circles) was bleached as described above in a HeLa cell expressing GFP-Rab7. (e) Fluorescence intensity of the bleach region of the GFP-cav-1 β-expressing cell (green) and the GFP-Rab7-expressing HeLa cell (red). Note the difference in peak size showing that GFP-Rab7 diffuses much more rapidly into the bleach field than GFP-cav. (f) Fluorescence intensity of the entire GFP-cav-1 β (green) and GFP-Rab7–expressing (red) cell. The GFP-rab7 signal can be completely removed compared with a much more limited extraction of GFP-cav, in particular from caveolae (arrows in a and b). Bars, 20 μm.

epithelial cell lines. We found that the fusion proteins were correctly targeted to caveolae at the plasma membrane. Importantly, application of various photobleaching techniques revealed that caveolae are normally immobile plasma membrane domains kept in place by the actin cytoskeleton, and the calculated very low mobile fraction of caveolin is incompatible with a role of caveolae in constitutive endocytic membrane trafficking.

MATERIALS AND METHODS

Construction of Enhanced Green Fluorescent Protein (GFP) Vector

*Bam*HI (blunt)/*Pst*I caveolin-1 α and -1 β fragments were derived from the plasmids pAS2–1-cav-1-1-534 and pAS2–1-cav-1-94-534, respectively (Stahlhut and van Deurs, 2000) and subcloned into the *Xho*I (blunt)/*Pst*I sites of pEGFP-C3 (CLONTECH, Palo Alto, CA/BD Biosciences, San Jose, CA) to generate N-terminally tagged caveolin fusion proteins (GFP-caveolin). The GFP-Rab7 fusion protein was made as previously described (Bucci *et al.*, 2000a). The C-terminally tagged caveolin-1-GFP fusion protein was a kind gift of Drs. L. Pelkmans and A. Helenius.

Cell Culture and Transfection

HeLa, A431, and Madin-Darby canine kidney (MDCK) (strain II) cells were grown in T25 flasks (Nalge Nunc International, Naperville, IL) at 37°C and 5% CO_2 in DMEM, supplemented with 10% fetal calf serum (5% for MDCK), 2 mM glutamine, 10 U/ml penicillin, and 10 μg/ml streptomycin, all reagents from Invitrogen (Carlsbad, CA). For transfection and fluorescence microscopy, the cells were grown in 6-cm Petri dishes (Nalge Nunc International) with a 4-cm-diameter hole in the bottom covered by a round glass coverslip glued on with Epon. The cells were transfected with the plasmids by using Fugene (Roche Molecular Biochemicals, Indianapolis, IN) and used 22–30 h after addition of transfection medium. The HEPES medium used for all live recordings was made of 20 mM HEPES (H3375; Sigma, St. Louis, MO), 140 mM NaCl, 2 mM $CaCl_2 \cdot 2H_2O$, 1 mg/ml D-(+)-glucose monohydrate (art 8342; Merck, Copenhagen, Denmark), 10 mM KCl; 5 N NaOH was added for adjustment to pH 7.5.

Western Blot

Lysates of cells transfected with pEGFP-cav-1 were separated on 4–20% acrylamide gels (Novex, San Diego, CA) and transferred to polyvinylidene difluoride membranes. Recombinant GFP (CLONTECH) served as positive control for the anti-GFP antibody. Membranes were blocked with 5% skim milk (Bio-Rad, Hercules, CA) in phosphate-buffered saline (PBS), 0.05% Tween 20. Primary and secondary antibodies were applied in the same buffer as follows: polyclonal anti-GFP (Molecular Probes, Eugene, OR), diluted 1:500; polyclonal anti-caveolin-1 (Transduction Laboratories, Lexington, KY), diluted 1:3000; and HRP-swine-anti-rabbit (DAKO, Carpinteria, CA), diluted 1:3000. Between incubations, membranes were rinsed three times with 0.05% Tween 20 in PBS. Immunosignals were detected using enhanced chemiluminescence reagent exposing polyvinylidene difluoride membranes on Hyperfilm (Amersham Biosciences, Piscataway, NJ).

Fluorescence Recovery in Photobleaching (FRAP) Analysis

The confocal microscope used was a Zeiss LSM 510 confocal microscope equipped with a tempcontrol 37-2 stage, an Ar laser, and C-apochromat 40×/1,2 W corr and Plan apochromat 100×/1.4 oil Iris lenses. The 40× lens was used for analysis of the cells at lower resolution, and the 100× lens was used for analysis with high magnifications of the thin peripheral regions of the cells. Bleaching of the outlined regions of interest (ROIs) was done at 37°C with an open pinhole, with the 488-nm laser line at full power and full transmission for 1–7 s, depending on the number and size of the ROIs. Observation of recovery was done at full laser power and only 1% transmission, to avoid significant photobleaching. LSM 510 software, version 2.2, was used to measure pixel intensity in the ROIs. The recovery values were normalized by dividing by the mean of

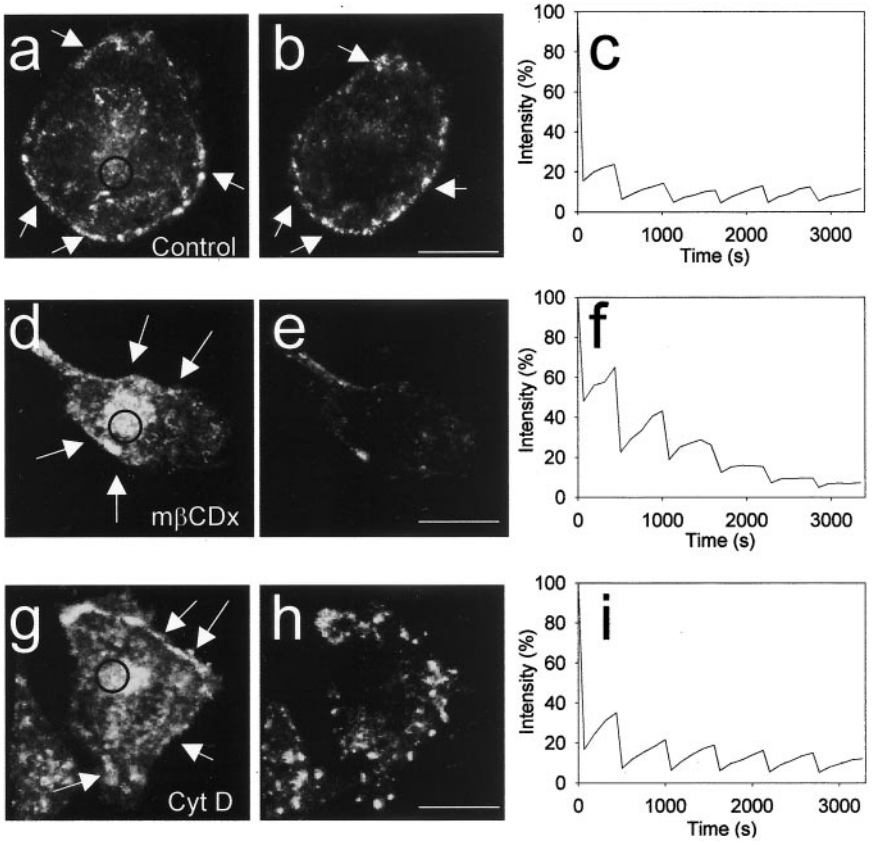

Figure 3. 4D FLIP analysis of GFP-cav–expressing cells treated with cyclodextrin and cytochalasin. (a and b) 3D reconstructions of a GFP-cav-1 β-expressing HeLa cell immediately before the first of six bleachings (the bleach region is indicated with a circle), and by the end of the experiment, after ~60 min. (c) Fluorescence intensity of the bleach region. Note that very little fluorescence diffuses into the bleach region after the first bleaching and that the appearance of caveolae (arrows in a and b) is largely unchanged even after 1 h. (d and e) A parallel experiment, in which 10 mM methyl-β-cyclodextrin was added 10 min before the first bleaching. See 4D movie Figure 3, d and e, in the online version. (f) Fluorescence intensity of the bleach region is shown. Note that caveolin here diffuses faster into the bleach region than in the control and that caveolae (arrows in d) disappear over time. (g and h) Experiment in which 10 μg/ml cytochalasin D was added 10 min before the first bleaching. See 4D movie Figure 3, g and h, in the online version. (i) Fluorescence intensity of the bleach region. Note that the normal caveolar pattern (arrows in g) is changed after cytochalasin treatment and that the fluorescence moves into the bleach region more efficiently than in the control. Bars, 20 μm.

prebleach values for each ROI and multiplying by 100. The half time required for the bleached fluorescence to rise to 50% of the full recovery value ($t_{1/2}$) and mobile fractions (M_f) were estimated by nonlinear regression to a function for lateral diffusion, as described (Yguerabide *et al.*, 1982). Statistica 2000 (Statsoft, Tulsa, OK) was used for the nonlinear regression, and Excel 97 (Microsoft, Redmond, WA) was used for subsequent calculation of the diffusion coefficient (D).

Four-dimensional (4D) Fluorescence Loss in Photobleaching (FLIP) Analysis

Image stacks of the cells were made with intervals of 2 min and consisted each of 10 confocal images. They were acquired using a pinhole diameter of 220 μm. Repeated bleachings were done every 10 min at full laser power and full transmission for each plane to obtain a uniform bleach cylinder through the cell. Observation of fluorescence loss and subsequent recovery was done at full laser power and only 1% transmission, to avoid significant photobleaching. The stacks were merged using the LSM 510 software. The resulting three-dimensional (3D) images were combined into 4D movies by using GIF Movie Gear 2.61 from Gamani productions. The relative fluorescence intensities over time were calculated from the sum of intensities of the ROIs in each stack by using the LSM 510 software in combination with Excel 2000 from Microsoft. The stacks covered the complete z-plane of the cells, eliminating out-of-focus signals.

Immunofluorescence Microscopy

Cells were washed twice in PBS, fixed for 30 min in 2% formaldehyde in phosphate buffer, washed in PBS, permeabilized in incubation buffer consisting of 5% normal goat serum and 0.2% saponin in PBS, and finally exposed to primary and secondary antibodies with washes in-between. The primary antibodies were mouse monoclonal or rabbit polyclonal anti-caveolin-1 (Transduction Laboratories), diluted 1:100; rabbit polyclonal anti-caveolin-1 α (Santa Cruz Biotechnology, Santa Cruz, CA), diluted 1:100; mouse monoclonal anti-Lamp-1 (Developmental Studies Hybridoma Bank; H4A3), diluted 1:100; mouse monoclonal anti-transferrin receptor (Roche Molecular Biochemicals; B3/25), diluted 1:100; rabbit polyclonal Lamp-1, a kind gift of Dr. S. Carlsson (Umeå University, Umeå, Sweden), diluted 1:500; and rabbit-anti-TGN-38 serum, a kind gift of Dr. M. McNiven (Mayo Clinic, Rochester, MN), diluted 1:100. Secondary antibodies were Alexa 488- or Alexa 568-conjugated anti-mouse or anti-rabbit antibodies (Molecular Probes), diluted 1:300, or Cy5-conjugated anti-mouse or anti-rabbit antibodies (Amersham Biosciences), diluted 1:500. The microscope described for FRAP analysis was also used for immunofluorescence. In addition, the 543- and 633-nm lines from two He/Ne lasers were used.

Experiments with Cyclodextrin, Cytochalasin, Okadaic Acid, and Cycloheximide

Methyl-β-cyclodextrin, cytochalasin D, okadaic acid, and cycloheximide (all from Sigma) were used in concentrations of 10 mM, 10 μg/ml, 1 μM, and 10 μg/ml, respectively, in the HEPES medium. In some experiments, okadaic acid was used in 1.6× hypertonic HEPES medium (Parton *et al.*, 1994).

Immunogold Localization of GFP-Caveolin

Nontransfected and transfected cells grown as described above but in T25 flasks (Nalge Nunc International) were washed with PBS and

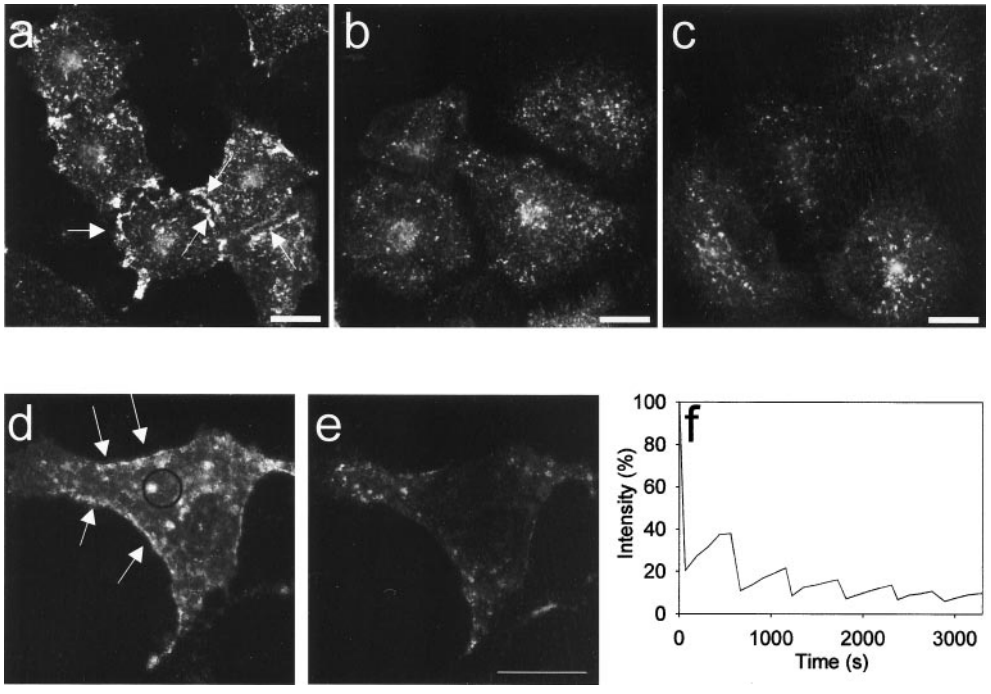

Figure 4. 3D reconstruction and 4D FLIP analysis of GFP-cav–expressing cells stimulated with okadaic acid. (a) 3D reconstruction of a control HeLa cell expressing GFP-cav-1 β, showing distinctly labeled caveolae (arrows). (b) GFP-cav-1 β-expressing HeLa cells stimulated for 1 h with 1 μM okadaic acid. Endocytosis of caveolae is seen. (c) Endocytosis of caveolae in GFP-cav-1 β-expressing HeLa cells treated for 1 h with 1 μM okadaic acid in 1.6$\times$ hypertonic medium. (d and e) 3D stacks from the beginning and the end of a FLIP experiment in which okadaic acid was added 10 min before the first bleaching. Distinct GFP-labeled cavolae are shown by arrows in d. These caveolae became internalized and were bleached within 1 h (e) because they readily moved into the bleach region (f). Bars, 20 μm.

fixed at room temperature in 0.1% glutaraldehyde and 2% formaldehyde in 0.1 M phosphate buffer pH 7.2. After a careful wash, the cells were scraped off the flasks, pelleted, and embedded in 7.5% gelatin in PBS. The pellets were incubated on ice with first 2.1 M sucrose and then 2.3 M sucrose, and frozen in liquid nitrogen. Ultrathin sections were cut on a Reichert Ultracut S microtome (Leica, Glostrup, Denmark), collected with 2.3 M sucrose, and mounted on Formvar-coated copper or nickel grids. Polyclonal anti-caveolin-1 (Transduction Laboratories) or polyclonal anti-GFP antibody (Molecular Probes) 1:50–1:100, followed by 10-nm protein A-gold 1:50–1:100 (purchased from Dr. G. Posthuma, Utrecht University, The Netherlands) were used to detect endogenous caveolin-1 and the GFP-cav-1 fusion proteins, respectively. Sections were analyzed in a Philips 100 CM electron microscope (Philips, Eindhoven, The Netherlands). Gold particles associated with caveolae and noncaveolar plasma membrane were counted in sections of cell pellets from at least two different experiments with either transfected or nontransfected cells. The number of caveolae per micrometer of plasma membrane was quantified in sections from three different experiments with transfected cells. Anti-GFP immunogold labeling was used to distinguish between transfected and nontransfected cells in these sections.

RESULTS

To analyze the dynamic properties of caveolae, we constructed two N-terminally tagged caveolin fusion proteins by using the enhanced version of GFP, GFP-caveolin-1 α (aa 1–178) and -1 β (aa 32–178), and expressed them in HeLa, A431, and MDCK cells. The functional differences between the two caveolin-1 isoforms, which both contain the essential caveolin scaffolding domain (aa 82–101) required for proper function, are unclear (Scherer *et al.*, 1995; Smart *et al.*, 1999; Fujimoto *et al.*, 2000; Schlegel and Lisanti, 2000;). Western blot analysis of lysates from GFP-caveolin–expressing cells with a polyclonal anti-GFP antibody revealed one single band of ~50 kDa (Figure 1a). Therefore, GFP-caveolin seemed to be maintained as a full-length fusion protein, allowing the tracing of the caveolin part of the fusion protein with the fluorescent GFP-signal. Because no appreciable differences in the localization or kinetic behavior between the two isoforms were obtained, we refer to both fusion proteins collectively as GFP-cav, unless otherwise specified. Moreover, because manipulations of the caveolin N-terminus may lead to impaired sorting of the protein to the plasma membrane and caveolae (Roy *et al.*, 1999; Pelkmans *et al.*, 2001) we also included a recently published C-terminally tagged caveolin-1 fusion protein (Pelkmans *et al.*, 2001), herein referred to as cav-GFP.

GFP-cav Is Correctly Sorted to Caveolae at Plasma Membrane

Expression of the fusion proteins resulted in a dotted staining at the plasma membrane being most distinct at the edges of the cells (Figure 1b). Moreover, a fluorescence signal was obtained from structures throughout the cytoplasm, although mainly concentrated in the perinuclear region. Although fluorescent structures at the edges appeared immobile, a proportion of the intracellular structures showed rapid movements.

After fixation of GFP-cav-1 β-transfected cells and subsequent immunofluorescence labeling for caveolin-1 α as a marker for endogeneous caveolin, a clear colocalization was obtained (our unpublished data). We also examined the colocalization of the intracellular GFP-cav signal with various markers of intracellular compartments. In this way, some colocalization of GFP-cav with both TGN-38 (a marker for the *trans*-Golgi network) and the transferrin receptor (a marker for early endosomes) was found, whereas only very

little colocalization of GFP-cav with Lamp-1 (a marker of late endocytic structures/lysosomes) was obtained (our unpublished data). In addition, some intracellular, GFP-cav–associated structures did not label for TGN-38, the transferrin receptor, or Lamp-1.

However, it was pertinent to the present study to localize the GFP-cav signal with high resolution, and we therefore used immunogold labeling with a polyclonal anti-GFP antibody. Very little apparently free cytosolic GFP-cav labeling was seen; virtually all gold particles were associated with membrane structures. Within the cells, some of these GFP-cav–associated membranes were part of the *trans*-Golgi network, some of the endosome system, and some of a tubulovesicular network. More importantly, at the cell periphery the GFP-cav labeling was almost exclusively associated with distinct caveolae close to the plasma membrane (Figure 1, c–f). Using ultracryosections of GFP-cav–transfected HeLa cells and the anti-GFP antibody followed by protein A-gold labeling, 85% of the gold particles (total 426 golds) associated with the plasma membrane were localized to caveolae. For comparison, in sections of nontransfected cells labeled with a polyclonal antibody against endogenous caveolin-1, the value was 92% (total 519 golds). Moreover, in transfected cells (identified by immunogold labeling with anti-GFP), 0.104 caveolae per micrometer of plasma membrane was found (total 107 caveolae), whereas in the neighboring nontransfected cells, 0.099 caveolae per micrometer was obtained (total 172 caveolae). Both in nontransfected and in transfected cells, caveolae typically appeared in patches separated by unlabeled caveolae-free plasma membrane. Taken together, these data show that the fluorescent dots seen at the edges of the GFP-cav-expressing cells correspond to caveolae and that the GFP-cav is correctly sorted to caveolae at the plasma membrane.

Integrity of GFP-cav and cav-GFP–associated Caveolae Depends on Cholesterol and an Intact Actin Cytoskeleton

The mobility of GFP-cav–associated caveolae in cells under standard culture conditions was analyzed by FLIP recordings in 4D (reconstructed stacks of 10 confocal sections covering the entire cell over time). We compared FLIP data obtained from GFP-cav–transfected cells with those from cells expressing GFP-Rab7. Rab7 is a small GTP-binding protein cycling between late endosomal/lysosomal membranes and the cytosol. It is involved in the formation and maintenance of the perinuclear aggregate of late endocytic structures (Bucci *et al.*, 2000a). Whereas only little fluorescence could be extracted from the GFP-cav–transfected cells, and most of this appeared to be from the intracellular pool of fluorescence because the strongly fluorescent caveolar rim of the cells was left unchanged, in the GFP-Rab7-transfected cells a very large amount of fluorescence diffused into the bleach region per bleaching cycle, and basically all fluorescence could be extracted (Figure 2). These experiments show that GFP-cav, in particular when associated with caveolae at the plasma membrane, is rather immobile.

Caveolae are cholesterol-based structures that disappear after cholesterol depletion with methyl-β-cyclodextrin (Chang *et al.*, 1992; Hailstone *et al.*, 1998; Rodal *et al.*, 1999). We therefore added methyl-β-cyclodextrin to GFP-cav- and cav-GFP–expressing cells. This caused a gradual disappearance of the strongly fluorescent dots and rims with fluorescent caveolin, leaving in the plasma membrane a diffuse GFP signal as seen in 4D reconstructions (Figure 3, d and e). To further visualize this effect of cholesterol depletion, we used FLIP to determine the mobility of caveolin in cholesterol-depleted cells compared with control cells. Whereas little fluorescence moved into the bleach field after each round of bleaching in untreated cells (parallel control experiment, Figure 3c), leaving the peripheral rim of caveolae intact (Figure 3, a and b), a much higher mobility was observed after cholesterol depletion as indicated by the steeper peaks of the FLIP curve (compare Figure 3, c and f).

It is known that depolymerization of the actin cytoskeleton with cytochalasin D results in clustering of caveolae that are still surface connected (Fujimoto *et al.*, 1995; van Deurs *et al.*, 1996). Moreover, it was recently shown that the actin-binding protein filamin is a ligand for caveolin-1, and that activation of Rho, which leads to a reorganization of the actin cytoskeleton, also causes a reorganization of caveolae (Stahlhut and van Deurs, 2000). This suggests that caveolae may normally be stabilized in the membrane by the actin cytoskeleton. After cytochalasin D-treatment of GFP-cav–expressing cells, the normal fluorescent caveolar pattern was disrupted and caveolae began to move laterally and cluster in the plasma membrane (Figure 3, g and h). An increased caveolae mobility was also reflected by the relatively large and steep peaks on the FLIP curve (Figure 3i). Similar results were obtained with cells expressing cav-GFP (our unpublished data). Taken together, these results show that GFP-cav- and cav-GFP–labeled caveolae behave like caveolae that are based on endogenous caveolin, and that they are quite stable under standard conditions.

Okadaic Acid Stimulates Endocytosis of GFP-cav and cav-GFP–associated Caveolae

It has previously been reported that treatment of cells with okadaic acid, in particular in combination with hypertonic medium, leads to endocytosis of caveolae (Parton *et al.*, 1994). To test whether this important feature of caveolae was preserved when using the N-terminally tagged caveolin construct, we compared the organization of GFP-cav–labeled caveolae in 3D reconstructions of untreated cells and of cells treated with okadaic acid in normal and in hypertonic medium. As seen in Figure 4, a–c, this treatment causes caveolae to disappear from the cell surface and aggregate in the perinuclear region. Moreover, the GFP-cav mobility was also increased as shown by FLIP analysis (Figure 4, d–f) and the repeated bleaching cycles led to an almost complete extraction of cellular fluorescence. Similar results were obtained with cav-GFP (our unpublished data).

GFP-cav- and cav-GFP–associated Caveolae Are Stable in Nonstimulated Cells

The striking immobility of the fluorescent caveolar compartment at the plasma membrane of unstimulated cells was further examined by bleaching the entire peripheral compartment to observe whether the fluorescence would recover, i.e., could be replaced by the fluorescence of the intracellular GFP-associated compartment, in which numerous vesicular structures moved around. No measurable ex-

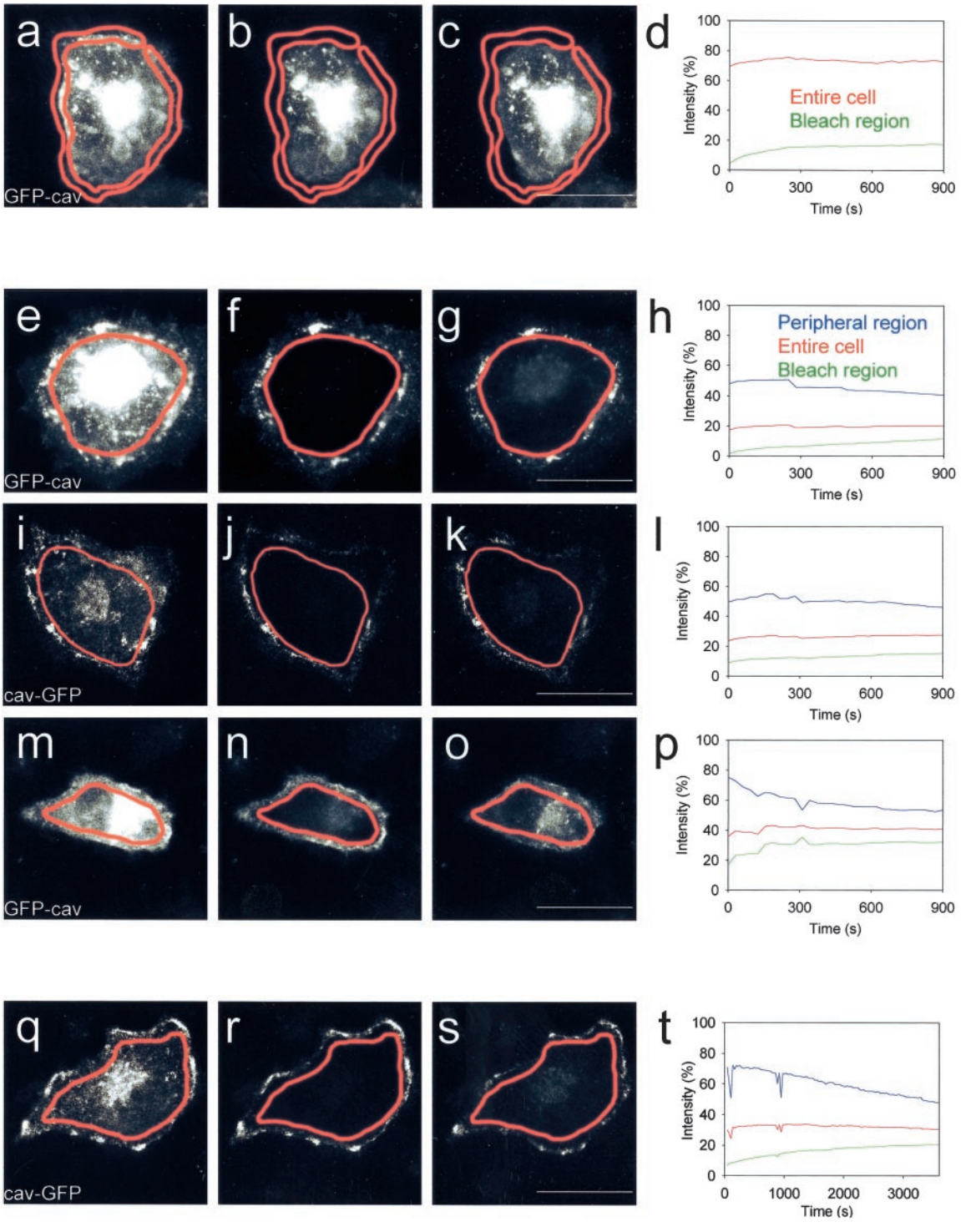

Figure 5. FRAP of the entire caveolar or intracellular GFP-cav and cav-GFP compartments of control cells and cells stimulated with okadaic acid. (a–c) Entire peripheral caveolar compartment (outlined in red) of a HeLa cell expressing GFP-cav-1 β was bleached. Images of the prebleach fluorescence, the fluorescence immediately after bleaching, and 15 min after bleaching is shown. See movie Figure 5, a–c, in the online version. (d) Fluorescence intensity in the peripheral bleach region (green) and of the entire cell (red) after bleaching. (e–g) Intracellular caveolin compartment of a GFP-cav-1 β-expressing HeLa cell was bleached (outlined in red). Images of the prebleach fluorescence, the fluorescence immediately after bleaching, and 15 min after bleaching is shown. See movie Figure 5, e–g, in the online version. (h) Fluorescence intensity of the bleach region (green), the nonbleached peripheral caveolae region (blue), and the fluorescence of the entire cell (red) after

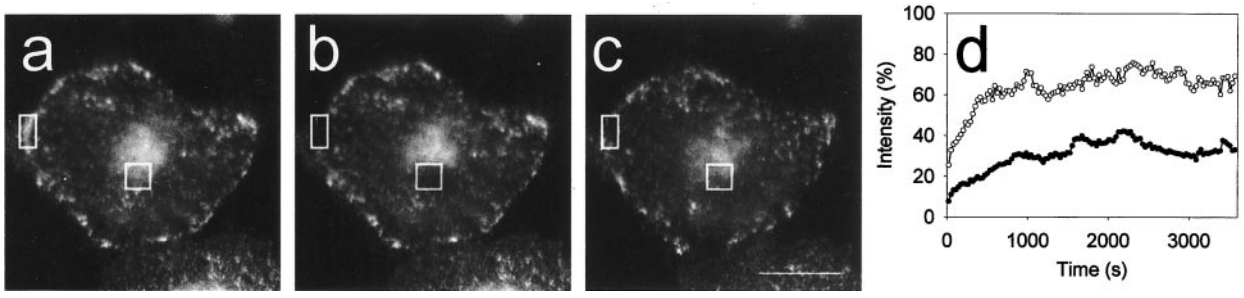

Figure 6. Example of FRAP analysis of intracellular and caveolae-associated cav-GFP. (a–c) Two bleach regions were selected in a cav-GFP–transfected HeLa cell, one in the cell periphery for GFP-labeled caveolae, and one for mainly intracellular, GFP-labeled structures in the perinuclear area. The two bleach regions are shown before bleaching (a), immediately after bleaching (b), and at the end of the experiment, after 1 h (c). (d) Fluorescence recovery curves from the same experiment are shown for caveolae (bottom curve) and intracellular structures (top curve). It is seen that the fluorescence associated with intracellular structures recovers much more efficiently than that associated with caveolae. Bar, 20 μm.

change took place, neither in HeLa cells transfected with GFP-cav (Figure 5, a–d) nor with cav-GFP (our unpublished data). The fluorescence of the peripheral region did not recover, and the level of intracellular fluorescence did not change, showing that no significant exchange took place between these two cellular compartments. Alternatively, the complete GFP-cav- and cav-GFP–associated intracellular compartment was bleached to see whether the remaining peripheral fluorescence would move to the interior of the cell. Only very little fluorescence recovery of the bleached intracellular compartment was observed (Figure 5, e–h and i–l), showing that very little exchange with the GFP-labeled, peripheral caveolar compartment took place. Similar results were obtained using A431 and MDCK cells transfected with GFP-cav (our unpublished data). Experiments with cycloheximide showed that the recovery of fluorescence of the bleached intracellular compartment was partly due to a very low level of caveolin internalization, partly due to new synthesis of GFP-labeled caveolin (our unpublished data). When the cells were treated with okadaic acid, the peripheral rim of caveolae clearly moved into the bleached interior of the cell (Figure 5, m–p).

Because the cells often tended to move, we preferred relatively short experimental times, e.g., 15 min, as used in the experiments shown in Figure 5, a–p. In cases where the cells did not move significantly, it was indeed possible to follow the fluorescence recovery after bleaching for longer periods of time, as shown in Figure 5, q–t.

Figure 5 (cont). bleaching. (i–l) Intracellular caveolin compartment of a cav-GFP–expressing HeLa cell was bleached (outlined in red). Images and fluorescence intensities presented as in e–h. Note that only very limited exchange of fluorescent material takes place between the caveolar and the intracellular compartment in the control cells shown in a–l. (m–p) Intracellular caveolin compartment of a GFP-cav-1 α-expressing HeLa cell treated with 1 μM okadaic acid was bleached (outlined in red). Okadaic acid was added 10 min before the bleaching. Images and fluorescence intensities presented as in e–h. See movie Figure 5, m–o, in the online version. Note that okadaic acid clearly induces internalization of caveolae. (q–s) Intracellular caveolin compartment of a cav-GFP–expressing HeLa cell (outlined in red) was bleached and the cell followed for 1 h. Images of the prebleach fluorescence, the fluorescence immediately after bleaching, and 1 h after bleaching are shown. (t) Fluorescence intensity of the bleach region (green), the nonbleached peripheral caveolae region (blue), and the fluorescence of the entire cell (red) after bleaching. Bars, 20 μm.

Kinetics of Caveolae-associated and Intracellular Fluorescent Caveolin Are Different

We next used FRAP to quantify the kinetic properties of the caveolar and the intracellular GFP-cav and cav-GFP compartments simultaneously in the same living cell. One bleach region was placed on the patches and clusters of caveolae at the cell periphery, and another one on the intracellular, perinuclear compartment. Figure 6 shows an experiment with a cav-GFP–transfected cell where the fluorescence recovery was followed for 1 h. Figure 7, a–c, shows images from a FRAP recording during 15 min obtained from a GFP-cav–transfected HeLa cell. In both Figures 6, a–c, and 7, a–c, it is seen that although the GFP signal from the intracellular compartment recovers to a high degree, the caveolar compartment at the cell periphery shows much more limited recovery. Moreover, it was striking that strongly fluorescent, elongated stretches at the cell periphery next to the peripheral bleach region (Figure 7, a–c) maintained their high fluorescence level in the period after bleaching and did not move into the bleach region, suggesting that only little lateral diffusion of fluorescent caveolin or lateral movement of fluorescently labeled caveolae took place.

Figure 7, d–g, shows the FRAP curves resulting from experiments performed on HeLa, A431, and MDCK cells, after curve fitting of the means of 9–14 independent recordings for each cell type. From these curve fits, the mobile fractions (M_f for $t = \infty$) and diffusion coefficients (D) were extracted as previously described (see MATERIALS AND METHODS). The mobile fraction of the caveolar compartment was strikingly lower than that of the intracellular compartment (Figure 8, filled and open bars, respectively). The diffusion coefficient for the mobile fraction of the fusion proteins was in the same order of magnitude ($\sim 1.0 \times 10^{-10}$ $cm^2\ s^{-1}$) at the cell periphery and within the cell. It should be noted that it may be inappropriate to use the term diffusion coefficient about data obtained for intracellular caveolin, because part of the movement of caveolin is not true

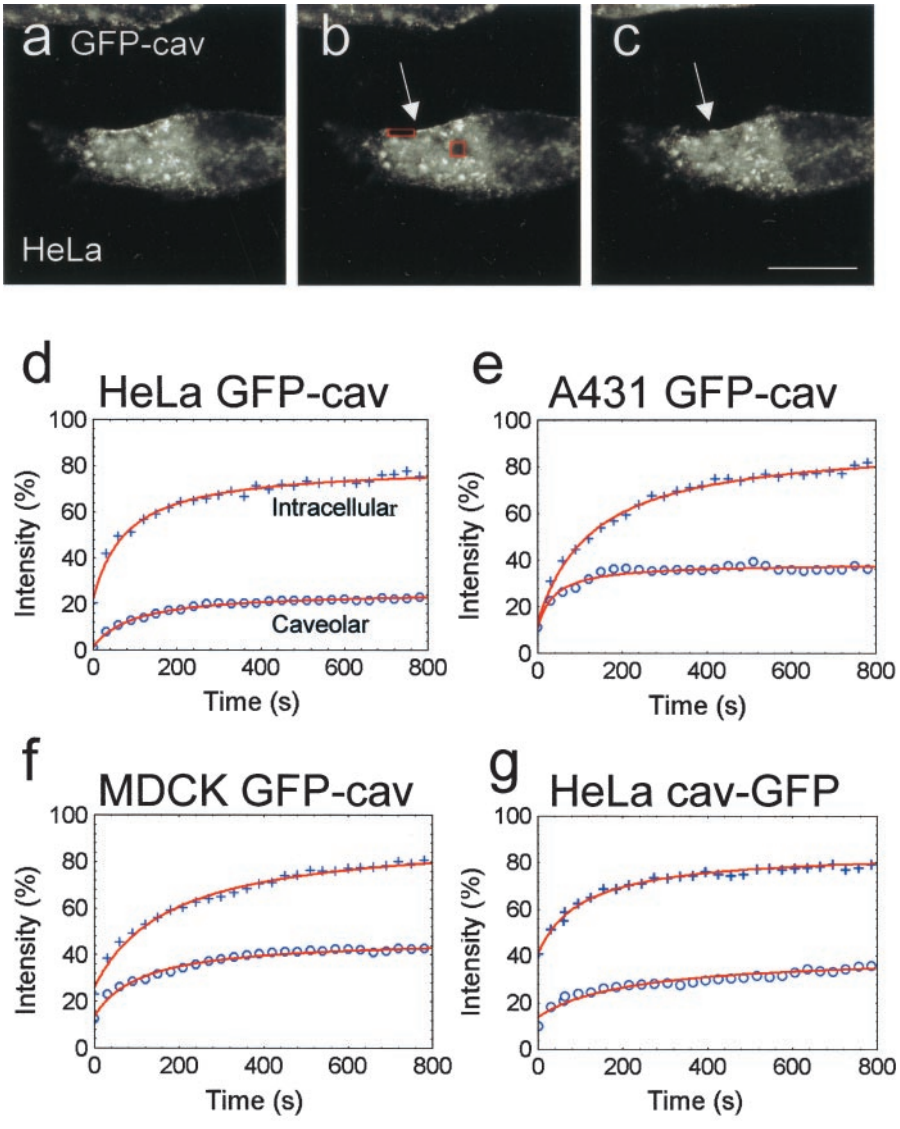

Figure 7. FRAP analysis of intracellular and caveolae-associated GFP-cav. (a–c) Bleach regions selected as in Figure 6 on a GFP-cav-1 β transfected HeLa cell. The two bleach regions are shown before bleaching (a), immediately after bleaching (b), and at the end of the experiment, after ~15 min (c). See movie Figure 7, a–c, in the online version. Note that the strongly fluorescent caveolar rim adjacent to the peripheral bleach region (arrows in b and c) appears unchanged during the experiment. (d–g) Curve fits of mean values of fluorescence intensities in the bleach regions of fluorescent intracellular structures and caveolae, respectively, within the first 800 s, obtained from 9 to 14 cells per experiment (+, intracellular fluorescence; o, caveolar fluorescence). Values have been normalized (% of prebleach values). It is seen that for all cell types and fusion proteins, the intracellular recovery is much more efficient than the caveolar recovery. Bar, 20 μm.

lateral diffusion, but due to active transport of caveolin-containing vesicles. It would therefore be more correct to interpret these recovery data as a "mobility coefficient."

Caveolae-associated GFP-cav and cav-GFP Represent a Largely Immobile Fraction of Fusion Protein

It should be stressed that the mobile fraction obtained for GFP-tagged caveolin associated with caveolae at the cell periphery most likely was overestimated in the above-mentioned experiments. In addition to caveolae, the peripheral bleach regions include some peripheral cytoplasm containing GFP-labeled vesicles with a mobility comparable to that of the intracellular compartment. In several of the bleach movies, it was evident that a weakly fluorescent area immediately below the strongly fluorescent rim of the cell actually recovered rapidly, whereas the rim itself remained largely without fluorescence.

It was therefore intended to analyze the kinetics of the GFP-cav- or cav-GFP–associated caveolar compartment with as little interference as possible from structures in the cytoplasm beneath. It was also relevant to further evaluate possible lateral diffusion in the plasma membrane. For this purpose, five different, small bleach regions were applied to the most peripheral GFP-cav- or cav-GFP–labeled rim of each cell for short-time micro-FRAP analysis (Figure 9, a–c). Five individual cells in each experiment (five FRAP regions per cell) were included. As expected, only very little recovery in these regions was observed after bleaching (Figure 9, d–k), and the calculated mobile fraction (for $t = \infty$) was as low as 5–20% (Figure 8, hatched bars). With this approach, the diffusion coefficient for the mobile fraction of GFP-labeled caveolae was found to be $\sim 0.3 \times 10^{-10}$ cm^2 s^{-1}.

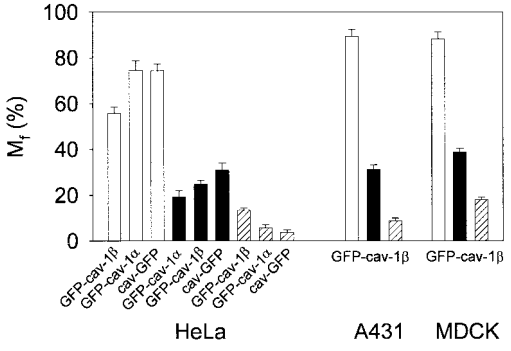

Figure 8. Mobile fractions (M_f) of intracellular and caveolae-associated caveolin fusion proteins. M_f values for GFP-cav-1 β and cav-GFP, calculated for $t = \infty$, are based on the curve fits shown in Figure 7. The values for GFP-cav-1 α are based on similar curve fits. M_f for intracellular fluorescent structures are shown with open bars, and for caveolae-associated fluorescence with filled bars. Moreover, M_f values for caveolae-associated GFP-cav-1 β and cav-GFP, based on the micro-FRAP experiments shown in Figure 9, as well as from micro-FRAP experiments with GFP-cav-1 α in HeLa cells, have been included (hatched bars). SD is indicated by error bars.

Measurements of the total fluorescence of the elongated stretches containing the five bleach regions showed that no change in fluorescence intensity took place after bleaching. FRAP analysis of bleach regions of the same size within the cell typically revealed a fluorescence recovery so fast that the drop in fluorescence immediately after bleaching could hardly be monitored (our unpublished data).

DISCUSSION

A combination of electron microscopical immunogold labeling and confocal microscopy demonstrated that the N-terminally tagged caveolin fusion proteins, GFP-cav-1 α and -1 β, used in the present study behaved as endogenous caveolin-1. Thus, the fusion proteins were sorted to the plasma membrane where the same proportion became associated with caveolae as for endogenous caveolin. Moreover, the number of caveolae in the transfected cells and in control cells was the same. The integrity of the fluorescently labeled caveolae depended on cholesterol, and cholesterol-depletion caused disappearance of caveolae as in nontransfected cells (Chang *et al.*, 1992; Hailstone *et al.*, 1998; Rodal *et al.*, 1999). Depolymerization of the actin cytoskeleton with cytochalasin D led to clustering of caveolae which, however, remained surface-connected, as also reported for caveolae in nontransfected cells (Fujimoto *et al.*, 1995; van Deurs *et al.*, 1996). Treatment of the transfected cells with okadaic acid stimulated endocytosis of caveolae as also reported for nontransfected cells (Parton *et al.*, 1994). Finally, the N-terminally tagged fusion proteins behaved in all respects like a C-terminally tagged caveolin fusion protein, cav-GFP, recently reported to allow simian virus 40-stimulated caveolar endocytosis (Pelkmans *et al.*, 2001).

The existence of motile, intracellular, fluorescent vesicles with a relatively high mobile fraction supports the general view that some intracellular caveolin-1–associated (caveolae-like) vesicles are involved in dynamic trafficking between the various caveolin-associated, intracellular compartments. However, once arrived at the plasma membrane, caveolin-1 is highly immobile under normal (standard culture) conditions and shows very limited exchange with the intracellular pool or lateral diffusion as evidenced by the decreased mobile fraction and diffusion coefficient (Lippincott-Schwartz *et al.*, 2001). In fact, this behavior of caveolin resembles that of E-cadherin. Thus, the mobile fraction of E-cadherin in cell-cell contact-free areas or in newly formed contacts is very high ($> 90\%$). However, when E-cadherin becomes trapped by the actin cytoskeleton to form either immobile punctate aggregates or plaques, the mobile fraction drops to $\sim 50\%$ and $< 10\%$, repectively (Adams *et al.*, 1998). The diffusion coefficients we obtained for the mobile fraction of caveolin by FRAP ($1 \times$ and 0.3×10^{-10} cm^2 s^{-1}, depending on the approach) are also in the same order of magnitude as that reported for E-cadherin (3.6×10^{-10} cm^2 s^{-1} [Adams *et al.*, 1998]; $\sim 0.3 \times 10^{-10}$ cm^2 s^{-1} [Kusumi *et al.*, 1993]). Thus, with respect to immobility caveolae resemble junctional complexes.

The demonstrated very low mobile fraction of caveolin associated with caveolae is incompatible with a role of caveolae in constitutive endocytic trafficking like that mediated by clathrin-coated pits and vesicles. Indeed, a very infrequent (but constitutive) internalization of caveolae cannot be excluded. On the basis of gold-labeling experiments, it has been calculated that formation of a new clathrin-coated pit takes place within 28 s, and that the entire population of coated pits at the cell surface is turned over in ~ 6 min (De Bruyn and Cho, 1987). Recent studies based on expression of GFP-clathrin and GFP-mHip1R (an actin-binding component of clathrin-coated pits) have similarly shown that clathrin-coated pits are highly mobile structures (Engqvist-Goldstein *et al.*, 1999; Gaidarov *et al.*, 1999; Damer and O'Halloran, 2000). Thus, within a given plasma membrane area, coated pits have very short lifetimes, disappearing and reappearing within seconds, and thereby maintaining a steady-state population. There seems to be only a very little, if any, immobile fraction of coated pits at the plasma membrane.

Although caveolae are not involved in constitutive endocytosis, internalization of these plasma membrane specializations can be stimulated in various ways, as mentioned in the INTRODUCTION. Caveolae have a tendency to cluster and fuse, and apparently also the capability to pinch off, processes that may depend on specific events leading to activation or assembly of the required molecular machinery, and which must be under tight control (Schnitzer *et al.*, 1995, 1996; Henley *et al.*, 1998; Oh *et al.*, 1998; Gilbert *et al.*, 1999). Our recent findings that the actin-binding protein filamin is a ligand for caveolin-1, and that Rho-activation and formation of actin stress-fibers reorganize caveolae (Stahlhut and van Deurs, 2000), and the present results showing that treatment of cells with cytochalasin D leads to increased mobility and clustering of caveolae, suggest that the actin cytoskeleton could play a key role in controlling the activity of caveolae and keeping them in place. Moreover, the endocytic potential of caveolae may be related to the specific cell type, a notion that is relevant in particular when considering cells and tissues in situ. There is, for instance, no direct evidence that caveolae become internalized in adipocytes, one of the cell types with most caveolae. On the other hand, caveolae in

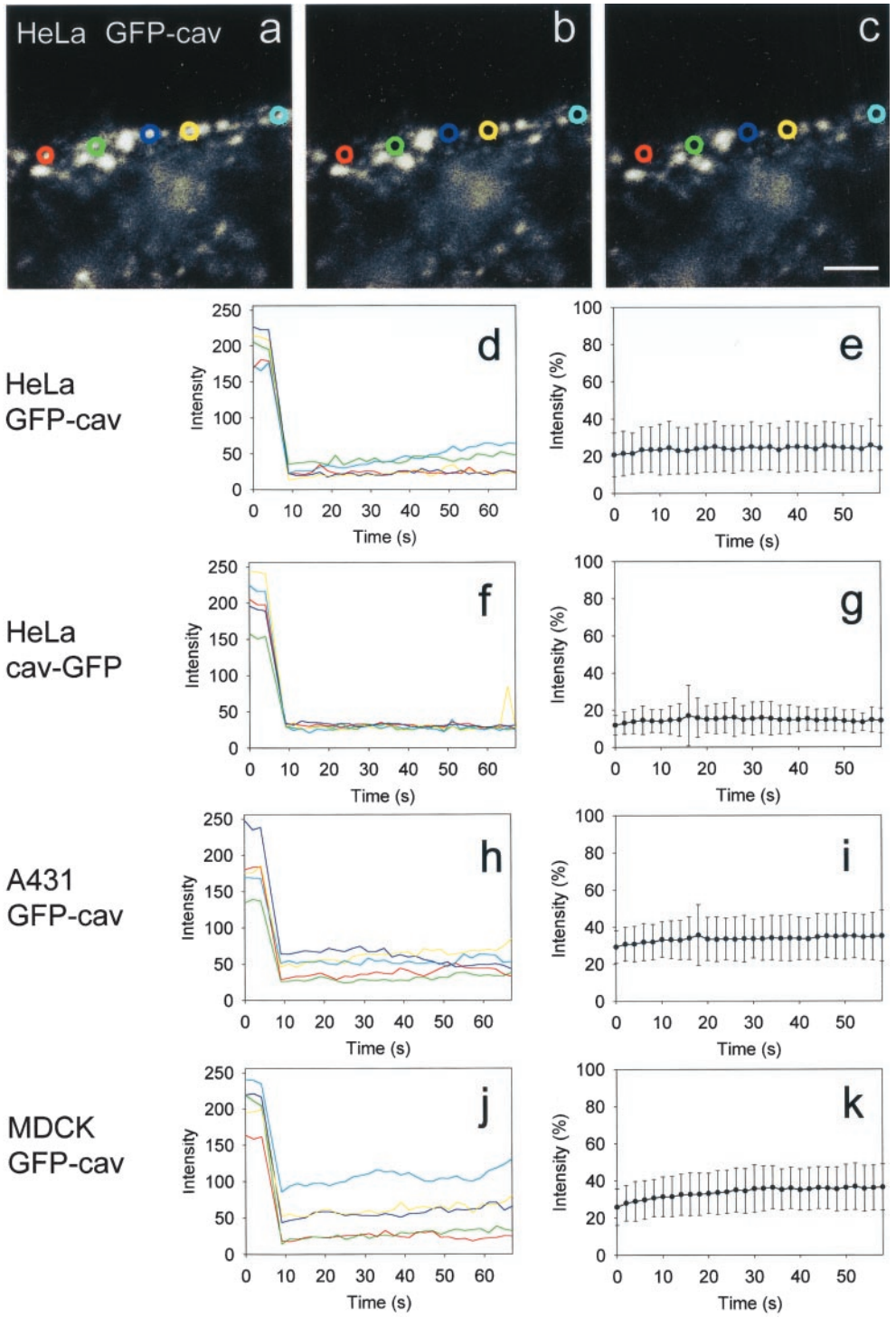

Figure 9. Micro-FRAP analysis of caveolae-associated GFP-cav and cav-GFP. (a–c) Five small bleach regions, indicated with different colors, were placed on the peripheral, fluorescent caveolar rim of a GFP-cav-1 β-transfected HeLa cell. The first image (a) represents the prebleach situation, the next image (b) the situation immediately after bleaching, and the last one (c) the end of the experiment after 1 min. See 4D movie Figure 9, a–c, in the online version. (d, f, h, and j) Absolute fluorescence intensities for the experiment with HeLa cells shown in a–c, as well as for a similar experiment with a cav-GFP–transfected HeLa cell, and with GFP-cav-1 β-transfected A431 and MDCK cells, respectively. The colors correspond to the five bleach regions used. (e, g, i, and k) Corresponding, normalized fluorescence intensity in the bleach regions after bleaching (mean $\pm$ SD, n = 25 for each experiment). Bar, 2 μm.

endothelial cells, which represent another cell type with large amounts of caveolae, are involved in transendothelial transport of albumin. Thus, the interaction of the albumin-docking protein pg60 with caveolin-1 and subsequent activation of downstream G_i-coupled Src kinase signaling triggers pinching off of endothelial caveolae (Minshall *et al.*, 2000). In endothelial cells, the often very short distance between the luminal and the abluminal surfaces (often a few hundred nanometers only) and the clear tendency of caveolae to form surface-connected, racemose clusters in these cells, may facilitate caveolae-mediated transendothelial transport. Hence, a tightly controlled fusion and fission activity between the individual components of the racemose caveolar clusters attached to either the lumenal or the abluminal surfaces could lead to efficient transendothelial transport with only little, if any, caveolar mobility.

In conclusion, our data indicate that caveolae under normal (standard culture) conditions represent a largely immobile plasma membrane compartment not involved in constitutive endocytosis. The immobility depends on an intact actin cytoskeleton. Under physiological conditions, stable caveolae at the plasma membrane may serve different functions, for instance, as key sensors and regulators of cholesterol homeostasis, as specialized, raft-like platforms facilitating the protein–protein interactions required for signaling to take place in response to changes in the cellular microenvironment, or for sequestration of inactive receptors.

ACKNOWLEDGMENTS

We thank Ulla Hjortenberg, Mette Ohlsen, and Keld Ottosen for technical assistance. We also thank Lucas Pelkmans and Ari Helenius for the kind gift of caveolin-GFP. This study was supported by grants to Bo van Deurs from the Danish Cancer Society, the Danish Medical Research Council, and the Novo Nordisk Foundation.

REFERENCES

Adams, C.L., Chen, Y.T., Smith, S.J., and Nelson, W.J. (1998). Mechanisms of epithelial cell-cell adhesion and cell compaction revealed by high-resolution tracking of E-cadherin-green fluorescent protein. J. Cell Biol. *142*, 1105–1119.

Anderson, R.G.W. (1998). The caveolae membrane system. Annu. Rev. Biochem. *67*, 199–225.

Bucci, C., Thomsen, P., Nicoziani, P., McCarthy, J., and van Deurs, B. (2000a). Rab7. A key to lysosome biogenesis. Mol. Biol. Cell *11*, 467–480.

Bucci, M., Gratton, J.-P., Rudic, R.D., Acevedo, L., Roviezzo, F., Crino, G., and Sessa, W.C. (2000b). In vivo delivery of the caveolin-1 scaffolding domain inhibits nitric oxide synthesis, and reduces inflammation. Nat. Med. *6*, 1362–1367.

Chang, W.J., Rothberg, K.G., Kamen, B.A., and Anderson, R.G.W. (1992). Lowering the cholesterol content of MA104 cells inhibits receptor-mediated transport of folate. J. Cell Biol. *118*, 63–69.

Damer, C.K., and O'Halloran, T.J. (2000) Spatially regulated recruitment of clathrin to the plasma membrane during capping, and cell translocation. Mol. Biol. Cell *11*, 2151–2159.

De Bruyn, P.P.H., and Cho, Y. (1987). Kinetic analysis of new formation, internalization, and turnover of bristle coated pits of the myeloid sinuses. Lab. Invest. *56*, 616–621.

Dessy, C., Kelly, R.A., Balligand, J.-L., and Feron, O. (2000). Dynamin mediates caveolar sequestration of muscarinic cholinergic receptors, and alteration in NO signaling. EMBO J. *19*, 4272–4280.

Engqvist-Goldstein, Å.E.Y., Kessels, M.M., Chopra, V.S., Hayden, M.R., and Drubin, D.G. (1999). An actin-binding protein of the Sla2/huntingtin interacting protein 1 family is a novel component of calthrin-coated pits and vesicles. J. Cell Biol. *147*, 1503–1518.

Fielding, C.J., and Fielding, P.E. (1997). Intracellular cholesterol transport. J. Lipid Res. *38*, 1503–1521.

Fielding, C.J., and Fielding, P.E. (2000). Cholesterol, and caveolae. structural and functional relationships. Biochim. Biophys. Acta *1529*, 210–222.

Fujimoto, T., Kogo, H., Ishiguro, K., Tauchi, K., and Nomura, R. (2001). Caveolin-2 is targeted to lipid droplets, a new. "membrane domain" in the cell. J. Cell Biol. *152*, 1079–1085.

Fujimoto, T., Kogo, H., Nomura, R., and Une, T. (2000). Isoforms of caveolin-1, and caveolar structure. J. Cell Sci. *113*, 3509–3517.

Fujimoto, T., Miyawaki, A., and Mikoshiba, K. (1995). Inositol 1,4,5-trisphosphate receptor-like protein in plasmalemmal caveolae is linked to actin filaments. J. Cell Sci. *108*, 7–15.

Gaidarov, I., Santini, F., Warren, R.A., and Keen, J.H. (1999). Spatial control of coated-pit dynamics in living cells. Nat. Cell Biol. *1*, 1–7.

Gilbert, A., Paccaud, J.P., Foti, M., Porcheron, G., Balz, J., and Carpentier, J.L. (1999). Direct demonstration of the endocytic function of caveolae by a cell-free assay. J. Cell Sci. *112*, 1101–1110.

Hailstone, D., Sleer, L.S., Parton, R.G., and Stanley, K.K. (1998). Regulation of caveolin and caveolae by cholesterol in MDCK cells. J. Lipid Res. *39*, 369–379.

Henley, J.R., Krueger, E.W.A., Oswald, B.J., and McNiven, M.A. (1998). Dynamin-mediated internalization of caveolae. J. Cell Biol. *141*, 85–99.

Huang, C.S., Zhou, J., Feng, A.K., Lynch, C.C., Klumperman, J., DeArmond, S.J., and Mobley, W.C. (1999). Nerve growth factor signaling in caveolae-like domains at the plasma membrane. J. Biol. Chem. *274*, 36707–36714.

Ikonen, E., and Parton, R.G. (2000). Caveolins, and cellular cholesterol balance. Traffic *1*, 212–217.

Isshiki, M., and Anderson, R.G. (1999). Calcium signal transduction from caveolae. Cell Calcium *26*, 201–208.

Kurzchalia, T.V., and Parton, R.G. (1996). And still they are moving. . . . Dynamic properties of caveolae. FEBS Lett. *389*, 52–54.

Kurzchalia, T.V., and Parton, R.G. (1999). Membrane microdomains and caveolae. Curr. Opin. Cell Biol. *11*, 424–431.

Kusumi, A., Yasushi, S., and Yamamoto, M. (1993). Confined lateral diffusion of membrane receptors as studied by single particle tracking (nanovid microscopy). Effects of calcium-induced differentiation in cultured epithelial cells. Biophys. J. *65*, 2021–2040.

Lippincott-Schwartz, J., Snapp, E., and Kenworthy, A. (2001). Studying protein dynamics in living cells. Nat. Rev. Mol. Cell Biol. *2*, 444–456.

Liu, P., Li., W.-P., Machleidt, T., and Anderson, R.G.W. (1999). Identification of caveolin-1 in lipoprotein particles secreted by exocrine cells. Nat. Cell Biol. *1*, 369–375.

Minshall, R.D., Tiruppathi, C., Vogel, S.M., Niles, W.D., Gilchrist, A., Hamm, H.E., and Malik, A.B. (2000). Endothelial cell-surface gp60 activates vesicle formation, and trafficking via Gi-coupled Src kinase signaling pathway. J. Cell Biol. *150*, 1057–1069.

Oh, P., McIntosh, D.P., and Schnitzer, J.E. (1998). Dynamin at the neck of caveolae mediates their budding to form transport vesicles

by GTP-driven fusion from the plasma membrane of endothelium. J. Cell Biol. *141*, 101–144.

Ostermeyer, A.G., Paci, J.M., Zeng, Y., Lublin, D.M., Munro, S., and Brown, D.A. (2001). Accumulation of caveolin in the endoplasmic reticulum redirects the protein to lipid storage droplets. J. Cell Biol. *152*, 1071–1078.

Parton, R.G. (1996). Caveolae and caveolins. Curr. Opin. Cell Biol. *8*, 542–548.

Parton, R.G., Joggerst, B., and Simons, K. (1994). Regulated internalization of caveolae. J. Cell Biol. *127*, 1199–1215.

Parton, R.G., and Lindsay, M. (1999). Exploitation of major histocompatibility complex class I molecules and caveolae by simian virus 40. Immunol. Rev. *168*, 23–31.

Pelkmans, L., Kartenbeck, J., and Helenius, A. (2001). Caveolar endocytosis of simian virus 40 reveals a new two-step vesicular transport pathway to the ER. Nat. Cell Biol. *3*, 473–483.

Pfeffer, S.R. (2001). Caveolae on the move. Nat. Cell Biol. *3*, E108–E110.

Pol, A., Luetterforst, R., Lindsay, M., Heino, S., Ikonen, E., and Parton, R.G. (2001). A caveolin dominant negative mutant associates with lipid bodies and induces intracellular cholesterol imbalance. J. Cell Biol. *152*, 1057–1070.

Ranzani, B., Schlegel, A., and Lisanti, M.P. (2000). Caveolin proteins in signaling, oncogenic transformation, and muscular dystrophy. J. Cell Sci. *113*, 2103–2109.

Rodal, S.K., Skretting, G., Garred, O., Vilhardt, F., van Deurs, B., and Sandvig, K. (1999). Extraction of cholesterol with methyl-β-cyclodextrin perturbs formation of clathrin-coated endocytic vesicles. Mol. Biol. Cell *10*, 961–974.

Roy, S., Luetterforst, R., Harding, A., Apolloni, A., Etheridge, M., Stang, E., Rolls, B., Hancock, J.F., and Parton, R.G. (1999). Dominant-negative caveolin inhibits H-Ras function by disrupting cholesterol-rich plasma membrane domains. Nat. Cell Biol. *1*, 98–105.

Scherer, P.E., Tang, Z., Chun, M., Sargiacomo, M., Lodish, H.F., and Lisanti, M.P. (1995). Caveolin isoforms differ in their N-terminal protein sequence and subcellular distribution. Identification and epitope mapping of an isoform-specific monoclonal antibody probe. J. Biol. Chem. *270*, 16395–16401.

Schlegel, A., and Lisanti, M.P. (2000). A molecular dissection of caveolin-1 membrane attachment and oligomerization. J. Biol. Chem. *275*, 21605–21617.

Schnitzer, J.E., Liu, J., and Oh, P. (1995). Endothelial caveolae have the molecular transport machinery for vesicle budding, docking, and fusion including VAMP, NSF, SNAP, annexins, and GTPases. J. Biol. Chem. *270*, 14399–14404.

Schnitzer, J.E., Oh, P., and MacIntosh, D.P. (1996). Role of GTP hydrolysis in fission of caveolae directly from plasma membranes. Science *274*, 239–242.

Shin, J.-S., and Abraham, S.N. (2001). Co-option of endocytic functions of cellular caveolae by pathogens. Immunology *102*, 2–7.

Shin, J.-S., Gao, Z., and Abraham, S.N. (2000). Involvement of cellular caveolae in bacterial entry into mast cells. Science *289*, 785–788.

Smart, E.J., Graf, G.A., McNiven, M.A., Sessa, W.C., Engelman, J.A., Scherer, P.E., Okamoto, T., and Lisanti, M.P. (1999). Caveolins, liquid-ordered domains, and signal transduction. Mol. Cell. Biol. *19*, 7289–7304.

Stahlhut, M., Sandvig, K., and van Deurs, B. (2000). Caveolae: uniform structures with multiple functions in signaling, cell growth, and cancer. Exp. Cell Res. *261*, 111–118.

Stahlhut, M., and van Deurs, B. (2000). Identification of filamin as a novel ligand for caveolin-1: evidence for the organization of caveolin-1-associated membrane domains by the actin cytoskeleton. Mol. Biol. Cell *11*, 325–337.

Stang, E., Kartenbeck, J., and Parton, R.G. (1997). Major histocompatibility complex class I molecules mediate association of SV40 with caveolae. Mol. Biol. Cell *8*, 47–57.

van Deurs, B., Holm, P.K., Sandvig, K., and Hansen, S.H. (1993). Are caveolae involved in clathrin-independent endocytosis? Trends Cell Biol. *3*, 249–251.

van Deurs, B., von Bulow, F., Vilhardt, F., Holm, P.K., and Sandvig, K. (1996). Destabilization of plasma membrane structure by prevention of actin polymerization. Microtubule-dependent tubulation of the plasma membrame. J. Cell Sci. *109*, 1655–1665.

van Meer, G. (2001). Caveolin, cholesterol, and lipid droplets? J. Cell Biol. *152*, F29–F34.

Wary, K.K., Mainiero, F., Isakoff, S.J., Marcantonio, E.E., and Giancotti, F.G. (1996). The adaptor protein Shc couples a class of integrins to the control of cell cycle progression. Cell *87*, 733–743.

Wary, K.K., Mariotti, A., Zurzolo, C., and Giancotti, F.G. (1998). A requirement for caveolin-1 and associated kinase Fyn in integrin signaling and anchorage-dependent cell growth. Cell *94*, 625–634.

Wei, Y., Yanf, X., Liu, Q., Wilkins, J.A., and Chapman, H.A. (1999). A role for caveolin and the urokinase receptor in integrin-mediated adhesion and signaling. J. Cell Biol. *144*, 1285–1294.

Yguerabide, J., Schmidt, J.M., and Yguerabide, E.E. (1982). Lateral mobility in membranes as detected by fluorescence recovery after photobleaching. Biophys. J. *39*, 69–75.